# FUSION OF HYPERSPECTRAL AND LIDAR DATA USING GENERALIZED COMPOSITE KERNELS: A CASE STUDY IN EXTREMADURA, SPAIN

*Mahdi Khodadadzadeh*[1], *Aurora Cuartero*[2], *Jun Li*[3], *Angel Felicísimo*[2] *and Antonio Plaza*[1]

[1]Hyperspectral Computing Laboratory, University of Extremadura, Cáceres, Spain
[2]Kraken Research Group, University of Extremadura, Cáceres, Spain
[3]School of Geography and Planning, Sun Yat-Sen University, Guangzhou, China

## ABSTRACT

The light detection and ranging (LiDAR) data provides very valuable information about the height of the surveyed area which can be used as a source of complementary information for the classification of hyperspectral data, in particular when it is difficult to separate complex classes. In this work, we suggest to exploit the generalized composite kernel strategy for fusion and classification of hyperspectral and LiDAR data. Our experimental results, conducted using a hyperspectral image and a LiDAR derived intensity image collected over a rural area in Extremadura, Spain, indicate that the proposed framework for the fusion of hyperspactral and LiDAR data provides significant classification results.

***Index Terms—*** Hyperspectral, light detection and ranging (LiDAR), generalized composite kernel, multinomial logistic regression (MLR), supervised classification.

## 1. INTRODUCTION

Remotely sensed image classification has been a very active area of research in recent years [1]. The goal of classification is to assign a unique label to each pixel given a set of observations. By recording hundreds of spectral bands, hyperspectral images have opened new possibilities in remote sensing image classification. In some cases, the data coming from other sources can be used to improve and/or refine hyperspectral image classification. A good example is the use of light detection and ranging (LiDAR) data [2], which can provide information about the height of the same surveyed area. LiDAR has been shown to be a very useful source of data for classification purposes [3]. In the literature, several techniques have been developed for fusion of hyperspectral and LiDAR data for classification purposes [4]. Techniques based on morphological features have been particularly successful for this purpose. For instance, the methodology in [5] jointly considered the features extracted by morphological attribute profiles [6] computed on both the hyperspectral and LiDAR data, and then fused the spectral, spatial and elevation information in a stacked architecture. In [7] it was pointed out that the simple concatenation or stacking of features such as morphological attribute profiles may contain redundant information. The main challenge in multiple feature learning is that how to adequately exploit the information containing in these features. In addition, a significant increase in the number of features may lead to high dimensionality issues that are in contrast with the limited number of training samples often available in remote sensing applications [8], which may lead to the Hughes effect. To address these issues, decision fusion techniques have been applied [9].

In this paper, we exploit composite kernels for the integration of hyperspectral and LiDAR data for classification purposes. The standard composite kernels and multiple kernel learning (MKL) methods based on support vector machines (SVMs) have shown a significant capacity to integrate multiple types of features [10]. Recently, in [11] a successful framework has been introduced for the development of generalized composite kernel machines for spectral-spatial hyperspectral image classification, which equally balances the spectral and the spatial information contained in the hyperspectral data without any weight parameters. A distinguishing feature of the method in [11] is that it uses the multinomial logistic regression (MLR) classifier, which naturally provides a probabilistic output and has a lot of flexibility in the construction of nonlinear kernels. In this work, we suggest to use MLR-based generalized composite kernel method for fusing spectral, spatial and height information derived from hyperspatral and LiDAR intensity images. Similar to [11], we consider morphological features as an important part of our framework with the difference that, here, we exploit the rich information provided by attribute profiles of the LiDAR intensity image in combination with the spectral information

available from the hyperspectral data. Our newly proposed approach is evaluated in a case study in which hyperspectral and LiDAR intensity images were collected over a rural area in Extremadura, Spain. The obtained results indicate that the proposed approach leads to good classification performance with very limited training samples.

## 2. METHODOLOGY

The proposed approach comprises two main steps. First, morphological feature extraction is performed from the LiDAR intensity image to produce a set of additional feature vectors. Then, the LiDAR-derived feature vectors and the spectral vectors from the original hyperspectral data are combined in a generalized composite kernel framework.

### 2.1. Feature Extraction

Let $\mathbf{X}^L \equiv (x_1^L, x_2^L, ..., x_n^L)$ be an intesity image derived from the LiDAR data, where $n$ is the number of pixels in $\mathbf{X}^L$. Similarly, let us denote the hyperspectral image as $\mathbf{X}^h \equiv (\mathbf{x}_1^h, \mathbf{x}_2^h, ..., \mathbf{x}_n^h)$, where $\mathbf{x}_i \in \mathbb{R}^d$, for $i = 1, 2, \ldots, n$, denotes a spectral vector, $n$ is the number of pixels in $\mathbf{X}^h$, and $d$ is the number of spectral bands. In order to perform feature extraction from the LiDAR data, we use morphological attribute profiles (APs) [12], which allow us to model different kinds of structural information. According to [13], APs of an intensity image $f$ arre built using morphological operations of thinning and thickening with a set of thresholds $\lambda_1$, $\lambda_2$, ..., $\lambda_n$ as follows:

$$AP(f_j(\mathbf{x}_i)) = \{\phi_n(f_j(\mathbf{x}_i)), ..., \phi_1(f_j(\mathbf{x}_i)), f_j(\mathbf{x}_i), \gamma_n(f_j(\mathbf{x}_i)), ..., \gamma_1(f_j(\mathbf{x}_i))\}, \quad (1)$$

where, $\phi$ and $\gamma$ denote the thickening and thinning transformations, respectively, and $f_j(\mathbf{x}_i)$ denotes a feature extracted from the original pixel information $\mathbf{x}_i$. Hence, by building the AP on the LiDAR intensity image $\mathbf{X}^l$, the LiDAR image based feature vectors $\tilde{\mathbf{X}}^L \equiv (\mathbf{x}_1^L, \mathbf{x}_2^L, ..., \mathbf{x}_n^L)$ are constructed, where $\mathbf{x}_i^L \in \mathbb{R}^{\tilde{d}}$ and $\tilde{d}$ is the dimension of the AP.

### 2.2. Classification Using Generalized Composite Kernels

Let $\mathbf{Y} \equiv (\mathbf{y}_1, \ldots, \mathbf{y}_n)$ denote an image of labels, $\mathbf{y}_i \equiv [y_i^{(1)}, y_i^{(2)}, \ldots, y_i^{(k)}]^T$, where $K$ is the number of classes. For $c = 1, \ldots, K$, if pixel $i$ belongs to class $c$, $y_i^{(c)} = 1$, otherwise, $y_i^{(c)} = 0$. Furthermore, let $\mathcal{D} = \{(\mathbf{x}_1, \mathbf{y}_1), \ldots, (\mathbf{x}_l, \mathbf{y}_l)\}$ represent the set of training samples. For classification of a pixel $\mathbf{x}_i$, the MLR models the posterior class probabilities as follows [14]:

$$p(y_i^{(c)} = 1 | \mathbf{x}_i, \boldsymbol{\omega}) = \frac{\exp(\boldsymbol{\omega}^{(c)^T} \boldsymbol{\phi}(\mathbf{x}_i))}{\sum_{c=1}^{K} \exp(\boldsymbol{\omega}^{(c)^T} \boldsymbol{\phi}(\mathbf{x}_i))}, \quad (2)$$

where $\boldsymbol{\omega}^{(c)}$ denotes the logistic regressors vector for class $c$, and $\boldsymbol{\omega} \equiv [\boldsymbol{\omega}^{(1)^T}, \ldots, \boldsymbol{\omega}^{(K)^T}]^T$; $\boldsymbol{\phi}(\mathbf{x}_i) \equiv [\phi_1(\mathbf{x}_i), \ldots, \phi_m(\mathbf{x}_i)]$ is a vector of $m$ fixed functions of the input, often termed as features. Based on the generalized composite kernel which have been proposed in [11], here we consider the input function $\boldsymbol{\phi}(\mathbf{x}_i)$ as:

$$\boldsymbol{\phi}(\mathbf{x}_i) = [1, K^h(\mathbf{x}_i^h, \mathbf{x}_1^h), \ldots, K^h(\mathbf{x}_i^h, \mathbf{x}_l^h), K^L(\mathbf{x}_i^L, \mathbf{x}_1^L), \ldots, K^L(\mathbf{x}_i^L, \mathbf{x}_l^L)]^T, \quad (3)$$

where $K^h$ and $K^L$ are spectral and LiDAR kernels, respectively. Similar to [11], we apply the logistic regression via a splitting and augmented Lagrangian (LORSAL) algorithm [15] to estimate the regressors for the MLR classifier.

## 3. EXPERIMENTAL RESULTS

Our experiments have been conducted for a pair of hyperspectral and LiDAR data collected over a rural area in Extremadura, Spain. The hyperspectral image was collected by a CASI sensor operated by Instituto Nacional de Tcnica Aeroespacial (INTA), and comprises 144 spectral bands in the range from 0.4 to 2.5 microns, with spatial resolution of 0,9m/1,66m (width/height). The LiDAR data were provided by Instituto Geogrfico Nacional (IGN) and was taken by an ASL60 LEICA Sensor. Fig. 1(a) shows a false color composite of the hyperspectral image, while Fig. 1(b) shows the LiDAR intensity image. Fig. 1(c) shows 6 classes of interest: *asphalt*, *soil*, *water*, *pathway*, *trees* and *buildings*. In order to test the performance of the proposed algorithms with limited training sets, 1% of the available labeled samples are used for training and the remaining samples are used for testing. For all classifiers, we optimized the necessary parameters and all the experiments are repeated 30 times. The average classification accuracies are reported. Table 1 shows the classification results obtained by the proposed approach. To have a complete comparison, the classification results obtained by our proposed method (MLR-GCK) are compared with those obtained by the traditional SVM [16] and the composite kernel-based SVM (SVK-CK) [10]. It is noticeable that the classification using multiple features (i.e. hyperspectral and LiDAR) improves the SVM classifier performance. For instance, SVM-CK approach obtained an overall accuracy (OA) of 94.51% and the MLR-GCK obtained an OA of 96.03%, which are respectively, 0.8 and 2.32% higher than

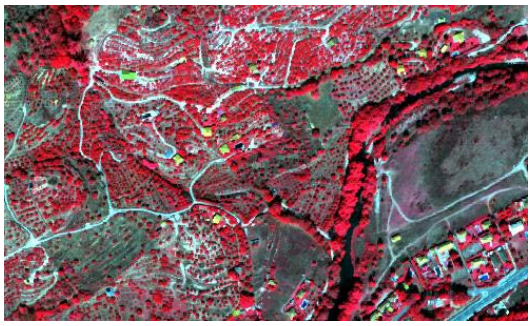

(a) Three-band false color image

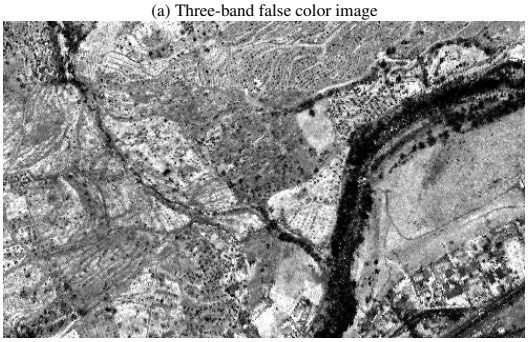

(b) LiDAR intensity image

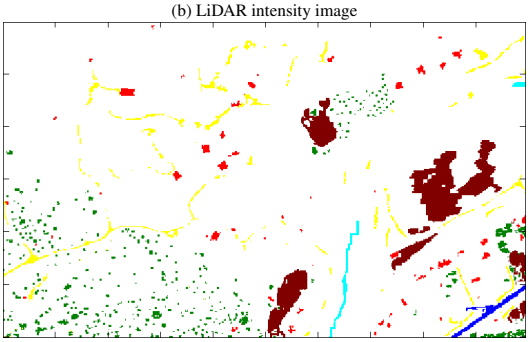

(c) The ground-truth map

**Fig. 1**. Hyperspectral and LiDAR data sets used in the study, along with the ground-truth map.

that obtained by the SVM classifier. Most importantly, the improvement for the classes *asphalt* and *water* using just 3 training samples per class is significant. Consequently, the improvement in obtained average accuracy (AA) for the composite kernel methods is more relevant. For instance, the MLR-GCK classifier improves the accuracy for the class *asphalt* by 31.09 %. Fig. 2 shows some of the obtained classification maps.

## 4. CONCLUSION

In this paper, we have exploited a generalized composite kernel strategy for fusion and classification of hyperspectral and LiDAR data. Our approach effectively integrates multiple

**Table 1**. Number of labeled samples and classification accuracies obtained by different methods.

| Class | Samples | | Classification methods | | |
|---|---|---|---|---|---|
| | Train | Test | SVM | SVM-CK | MLR-GCK |
| Asphalt | 3 | 382 | 65.05 | 93.36 | 96.14 |
| Soil | 55 | 5547 | 98.11 | 98.49 | 98.77 |
| Water | 3 | 345 | 85.05 | 99.29 | 97.47 |
| Pathway | 24 | 2450 | 94.97 | 93.58 | 94.21 |
| Trees | 23 | 2329 | 94.15 | 94.03 | 94.51 |
| Buildings | 10 | 1050 | 79.82 | 75.58 | 88.65 |
| OA | | | 93.71 | 94.51 | 96.03 |
| AA | | | 86.19 | 92.39 | 94.96 |
| $\kappa$ | | | 90.93 | 92.10 | 94.31 |

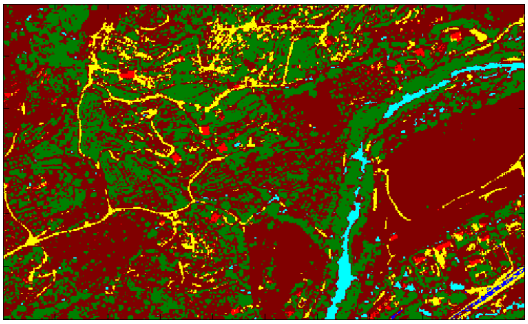

(a) SVM (92.46%, 84.19%)

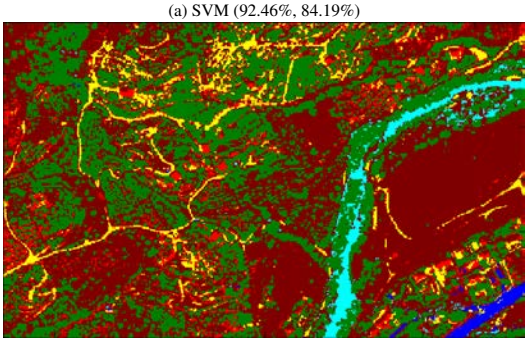

(b) SVM-CK (93.95%, 92.82%)

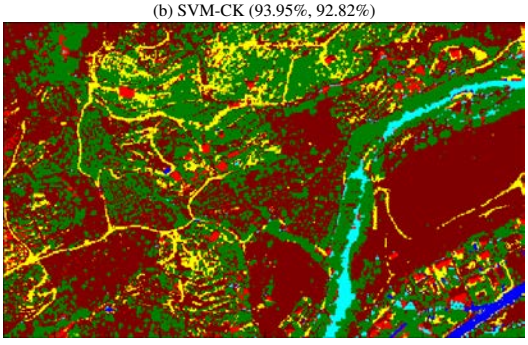

(c) MLR-GCK (95.33%, 94.95%)

**Fig. 2**. Classification maps and (overall, average) classification accuracies obtained by different methods.

types of features extracted from these data without the need for any regularization or weight parameters. We have considered several types of spatial and spectral features derived from the original hyperspectral image and from the LiDAR derived intensity image, including the full original spectral information and different types of morphological profiles calculated for the LiDAR data. Our experimental results, conducted using a hyperspectral image and a LiDAR derived image collected over a rural area in Extremadura, Spain, indicate that the information provided by LiDAR can effectively complement the spectral information from the hyperspectral data.

# References


[1] A. Plaza, J. A. Benediktsson, J. Boardman, J. Brazile, L. Bruzzone, G. Camps-Valls, J. Chanussot, M. Fauvel, P. Gamba, J. Gualtieri, M. Marconcini, J. C. Tilton, and G. Trianni, "Recent advances in techniques for hyperspectral image processing," *Remote Sensing of Environment*, vol. 113, pp. 110–122, 2009.

[2] H. Lee and N. Younan, "DTM extraction of LiDAR returns via adaptive processing," *IEEE Transactions on Geoscience and Remote Sensing*, vol. 41, no. 9, pp. 2063–2069, Sept 2003.

[3] J. Jung, E. Pasolli, S. Prasad, J. Tilton, and M. Crawford, "A framework for land cover classification using discrete return LiDAR data: Adopting pseudo-waveform and hierarchical segmentation," *IEEE Journal of Selected Topics in Applied Earth Observations and Remote Sensing*, vol. 7, no. 2, pp. 491–502, Feb 2014.

[4] H. Wang, C. Glennie, and S. Prasad, "Voxelization of full waveform LiDAR data for fusion with hyperspectral imagery," in *Proceedings of the IEEE International Geoscience and Remote Sensing Symposium*, July 2013, pp. 3407–3410.

[5] M. Pedergnana, P. Marpu, M. Dalla Mura, J. Benediktsson, and L. Bruzzone, "Classification of remote sensing optical and LiDAR data using extended attribute profiles," *IEEE Journal of Selected Topics in Signal Processing*, vol. 6, no. 7, pp. 856–865, Nov 2012.

[6] M. Dalla Mura, J. Benediktsson, B. Waske, and L. Bruzzone, "Morphological attribute profiles for the analysis of very high resolution images," *IEEE Trans. Geosci. Rem. Sens.*, vol. 48, no. 10, pp. 3747 –3762, Oct 2010.

[7] W. Liao, R. Bellens, A. Pizurica, S. Gautama, and W. Philips, "Graph-based feature fusion of hyperspectral and LiDAR remote sensing data using morphological features," in *Proceedings of the IEEE International Geoscience and Remote Sensing Symposium*, vol. 7, July 2013, pp. 4942–4945.

[8] S. Prasad and L. M. Bruce, "Overcoming the small sample size problem in hyperspectral classification and detection tasks," in *Proc. IEEE Int. Conf. Geosci. Remote Sens. (IGARSS)*, vol. 5, 2008, pp. 381–384.

[9] G. Licciardi, F. Pacifici, D. Tuia, S. Prasad, T. West, F. Giacco, J. Inglada, E. Christophe, J. Chanussot, and P. Gamba, "Decision fusion for the classification of hyperspectral data: Outcome of the 2008 GRS-S data fusion contest," *IEEE Trans. Geosci. and Remote Sens.*, vol. 47, no. 11, pp. 3857–3865, 2009.

[10] G. Camps-Valls, L. Gomez-Chova, J. Munoz-Mari, J. Vila-Frances, and J. Calpe-Maravilla, "Composite kernels for hyperspectral image classification," *IEEE. Geoscience and Remote Sensing Letters*, vol. 3, no. 1, pp. 93–97, Jan. 2006.

[11] J. Li, P. R. Marpu, A. Plaza, J. M. Bioucas-Dias, and J. A. Benediktsson, "Generalized composite kernel framework for hyperspectral image classification," *IEEE Transactions on Geoscience and Remote Sensing*, vol. 51, no. 9, pp. 4816–4829, 2013.

[12] M. Dalla Mura, J. Atli Benediktsson, B. Waske, and L. Bruzzone, "Morphological attribute profiles for the analysis of very high resolution images," *IEEE Transactions on Geoscience and Remote Sensing*, vol. 48, no. 10, pp. 3747 –3762, 2010.

[13] M. D. Mura, J. A. Benediktsson, B. Waske, and L. Bruzzone, "Extended profiles with morphological attribute filters for the analysis of hyperspectral data," *International Journal of Remote Sensing*, vol. 31, no. 10, pp. 3747–3762, Oct. 2010.

[14] D. Bohning, "Multinomial logistic regression algorithm," *Ann. Inst. Stat. Math.*, vol. 44, no. 1, pp. 197–200, 1992.

[15] J. Bioucas-Dias and M. Figueiredo, "Logistic regression via variable splitting and augmented lagrangian tools," Instituto Superior Tcnico, Lisbon, Portugal, Tech. Rep., 2009.

[16] C. Chang and C. Lin. (2009) LIBSVM: A library for support vector machines. [Online]. Available: http://www.csie.ntu.edu.tw/ cjlin/libsvm